IEEE Access
Multidisciplinary | Rapid Review | Open Access Journal

Received 27 November 2022, accepted 5 December 2022, date of publication 8 December 2022,
date of current version 13 December 2022.

Digital Object Identifier 10.1109/ACCESS.2022.3227625

RESEARCH ARTICLE

A Single-Carrier Delay-and-Superposition Based High Spectral Efficiency Differential Chaos Shift Keying for Maritime Internet of Vessels

XINYU DOU, TENGXIAO LYU, BAOJUN FAN, AND DEQUN LIANG
College of Information Science and Technology, Dalian Maritime University, Dalian 116026, China

Corresponding author: Xinyu Dou (xydou@dlmu.edu.cn)

This work was supported in part by the National Natural Science Foundation of China under Grant 62001077, in part by the China Postdoctoral Science Foundation Funded Project under Grant 2019M661075 and Grant 2022T150081, and in part by the Dalian High-Level Talent Innovation Support Plan under Grant 2021RQ063.

ABSTRACT The fast growing Internet of Vessels (IoV) requires maritime communications to be more spectral efficient to make full use of the scarce maritime spectral resource, provide a high data transmission rate and support massive communication nodes to access the network. However, the spectral efficiency of most existing maritime communications are still relatively low, and consequently maritime communications can hardly support high volume multi-user communications. Therefore, in this paper, a high spectral efficiency Differential Chaos Shift Keying system based on a single-carrier delay-and-superposition modulation technology (SCDS-DCSK) is proposed for IoV scenarios. In a SCDS-DCSK symbol, all sub-carriers have the same frequency, indicating that the symbol of SCDS-DCSK only occupies the bandwidth of a single sub-channel. As a result, a large amount of maritime communication resources can be saved for accommodating more communication nodes and the spectral efficiency is significantly improved. System architectures and principles are firstly demonstrated. Then, the spectral efficiency, peak mean power ratio (PAPR), complexity, and the origin of error bits of SCDS-DCSK are analyzed, and the bit-error-rate expressions are derived. Moreover, effects of various system parameters and levels of sea states on the system performance are simulated and discussed. Simulation results verify the theoretical analyses, and manifest that the SCDS-DCSK can achieve a high spectral efficiency under various sea states. Thanks to characteristics such as high spectral efficiency, flexible parameter configuration, and simple implementation, SCDS-DCSK is a promising technology for improving the quality of service (QoS) of future maritime IoV.

INDEX TERMS Chaotic communication, single-carrier delay-and-superposition, spectral efficiency, maritime communications, Internet of Vessels (IoV).

I. INTRODUCTION

As the expansion of Internet of Things (IoT) into the maritime domain, Internet of Vessels (IoV) enables massive connections among vessels, sailors and waterways, making maritime activities more intelligent, efficient and safe [1]. With the rapid development of IoV, existing maritime communications have faced huge challenges in spectral efficiency. Firstly, more maritime communication devices will be deployed in various maritime infrastructures such as wharfs, buoys, cargos and Unmanned Surface Vehicles (USVs) to transmit their specific information. As the maritime spectral resource is much scarcer than the terrestrial spectral resource, maritime communication urgently needs a more spectral efficient technology to support such a rapid growth of IoV communication devices. Secondly, the energy supply of maritime IoV nodes, such as USVs or buoys, is relatively tight. As a result, communication technologies of maritime IoV must be as simple as possible to ensure a low energy consumption. Therefore, it is necessary to develop a spectral

The associate editor coordinating the review of this manuscript and approving it for publication was Yi Fang.

efficient and meanwhile simple maritime communication technology for long-term and stable development of IoV and Smart Ocean.

Recently, chaos-based communication technologies, especially Differential Chaos Shift Keying (DCSK), is proved to be suitable for Internet of Things (IoT) scenarios, since DCSK not only inherits the high level of security, strong anti-jamming and anti-interception of the chaotic sequence, but also avoids complex chaos synchronization circuits at the receiver, indicating a simpler system implementation [2]. However, due to the transmitted-reference (T-R) structure, traditional DCSK suffers from a relatively low spectral efficiency and data transmission rate. Fortunately, thanks to various modern wireless communication technologies such as multi-carrier modulations and index modulations, etc., DCSK and its modified version can overcome above inherent drawbacks and achieve a higher spectral efficiency and data transmission rate. The concept of multi-carrier DCSK (MC-DCSK) was firstly demonstrated by G. Kaddoum, in which the chaotic reference and information-bearing signals are conveyed by different frequency sub-channels [3]. In this way, both the spectral efficiency and data transmission rate of DCSK are increased. A multiresolution M-Ary DCSK system was designed, in which a single chaotic carrier can carry multiple information bits via the constellation symbol [4], [5], [6]. Then, Huang et al. extended the M-Ary DCSK modulation to MC-DCSK to increase the data transmission rate of MC-DCSK [7]. Moreover, the Orthogonal Frequency Division Multiplexing (OFDM) technology is proposed to replace the traditional multi-carrier modulations [8], [9]. As a result, the spectral and energy efficiencies were both improved. In addition, a variety of index modulation (IM) technologies, such as carrier index or code index modulations, are introduced to MC-DCSK systems to increase the spectral efficiency through mapping more information bits into key parameters of the system [2], [10], [11], [12], [13].

What's more, high spectral efficiency DCSK systems can even support multi-access communications. Yi et al. demonstrated three kinds of multiple-access DCSK systems [14]. For instance, MU-DCSK based on Walsh codes distinguishes multiple users based on different Walsh codes. Kaddoum et al. studied the performance of traditional MC-DCSK in the multi-user scenario [15]. Then, they proposed the orthogonal frequency division multiplexing DCSK (OFDM-DCSK) for multi-user communications, in which chaotic reference signals occupied different subcarriers with different frequencies, and information bearing signals of all users shared other bandwidths [9]. Moreover, the network coding was deployed to further improve the performance of MU-DCSK [16]. A MU-PPM-DCSK based on superposition coding was proposed in [17], in which users were distinguished by different superposition codes. A MU-DCSK system based on sparse coding technology was proposed in [18], in which the information of a user mapped the information into a specific wavelength group. Through sparse coding technology, multiple users could share limited bandwidth, and the spectral efficiency of MU-DCSK were further improved.

Therefore, the high spectral efficiency DCSK is a promising technology for IoV because it can match well with demands of maritime IoV communications. As the spectral resource of the maritime domain is much scarcer than that of the terrestrial domain, DCSK must be more spectral efficient than ever to fully use the maritime spectral recourse and to allow more devices access to the IoV network. Therefore, in this paper, from the aspect of basic modulations, we have proposed a high spectral efficiency DCSK based on a novel single-carrier delay-and-superposition modulation technology (SCDS-DCSK), and analyzed its performance under various system parameters and sea states. At the transmitter of SCDS-DCSK, all subcarriers are gathered into a single frequency sub-channel through a novel Delay-and-Superposition modulation technology, which is inspired by [19] and [20]. In this way, the whole system achieves a significantly increased spectral efficiency. At the receiver, information bits are demodulated by solving a linear equation set constructed by sub-carriers. Main contributions of this paper are summarized as follows.

(1) A high spectral efficiency DCSK based on the single-carrier delay-and-superposition modulation is proposed. Principles of the transmitter and the receiver are demonstrated, and the spectral efficiency, PAPR, complexity and the bit error rate (BER) of the proposed system are analyzed.

(2) Effects of various system parameters on the system performance are simulated to verify the theoretical analysis. Then, system performance under different level of sea states is simulated, and some performance improving methods are discovered based on simulation results.

(3) Performance comparison between SCDS-DCSK and other typical DCSKs, such as the traditional MC-DCSK and OFDM-DCSK, are implemented under various sea states to demonstrate the superiority of the proposed system.

The reminder of this paper is organized as follows. Section II demonstrates the architecture and principle of SCDS-DCSK and demonstrates the maritime channel model. Section III analyzes the system performance, such as spectral efficiency, PAPR, complexity and the BER of SCDS-DCSK. Section IV presents the simulations and discussions. Finally, the conclusions are given in section V.

II. SYSTEM ARCHITECTURE AND PRINCIPLE

A. SINGLE-CARRER DELAY-AND-SUPERPOSITION MODULATION (SCDS) BASED DCSK

The transmitter of the SCDS-DCSK is shown in Fig. 1. M serial information bits (s_m, $m = 1, \ldots, M$) are firstly converted into M parallel paths of bits, and then they are spreaded by a chaotic reference signal. The chaotic reference signal is generated by the Logestic map $x_{k+1} = 1 - x_k^2$, where x_k and x_{k+1} represents the kth and $(k+1)$ th sample of the chaotic sequence. Afterwards, chaotic reference and

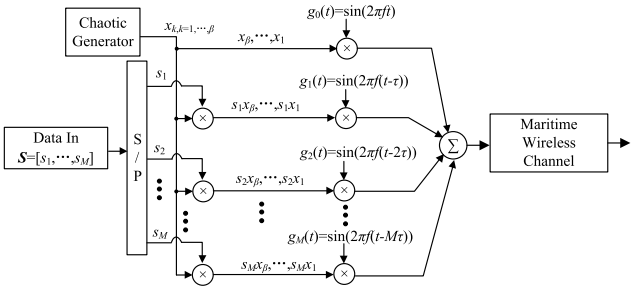

FIGURE 1. Principle of the transmitter of SCDS-DCSK.

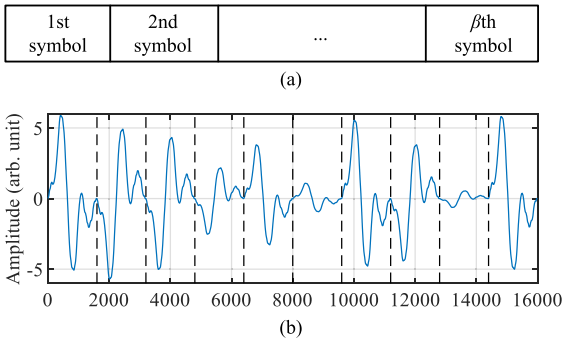

FIGURE 2. Frame format of SCDS-DCSK. (a) Frame structure of SCDS-DCSK. (b) Waveform of a SCDS-DCSK frame. β is set to be 10.

information bearing signals are modulated on $M+1$ sub-carriers. Sub-carriers of SCDS- DCSK are expressed as follows,

$$g_n(t) = \begin{cases} \sin(2\pi f(t - n\cdot\tau)), & t \in T \\ 0, & t \notin T \end{cases} \quad (1)$$

where $n = 0, \ldots, M$, and T is the duration of one subcarrier. Note that, sub-carriers of SCDS-DCSK have two remarkable characters:

1) All sub-carriers have the same frequency f;

2) There is a time delay τ between neighbor sub-carriers.

After carrier modulation, all modulated sub-carriers are directly superpositioned in time domain to construct the SCDS-DCSK symbol,

$$S_k(t) = \sum_{m=0}^{M} a_{mk} g_m(t), \quad (2)$$

where $k = 1, \ldots, \beta$, $a_{mk} = s_m x_k$, and $a_{0k} = x_k$ when m equals to 0. The format and waveform of an SCDS-DCSK frame is shown in Fig. 2. An SCDS-DCSK frame contains β symbols.

As all sub-carriers have the same frequency, this modulation technology actually belongs to the single carrier modulation, and the SCDS-DCSK symbol only occupies the bandwidth of a single frequency sub-channel. In this way, frequency recourses can be saved for accommodating more users and nodes. In addition, thanks to the credible digital system design, the time delay is easier to be implemented than that in the analog modulation scenario [21].

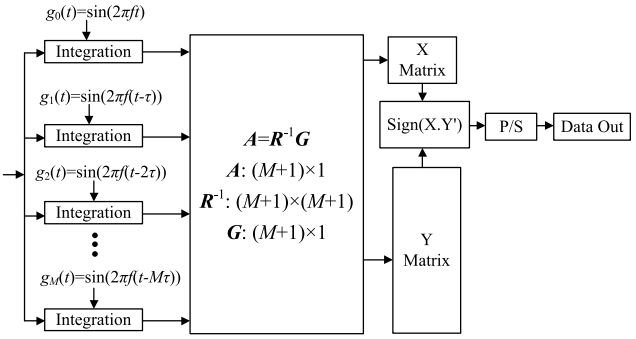

FIGURE 3. Principle of the receiver of SCDS modulation.

The receiver of SCDS-DCSK is shown in Fig. 3. As all subcarriers utilize the same frequency, traditional demodulation methods such as matched filters or fast Fourier transform (FFT) cannot be used to recover information bits. In SCDS-DCSK, an equation set about all information bits can be construct through coherent operations, and all information bits can consequently be obtained by solving this equation set. The demodulation process is detailed as follows.

Firstly, the coherent operation between the received signal and the undelayed sub-carrier is

$$\begin{aligned} G_{0k} &= \int_0^T \sin(2\pi ft) \times S_k(t)dt \\ &= \int_0^T \sin(2\pi ft) \times \{a_{0k}\sin(2\pi ft) \\ &\quad + a_{1k}\sin[2\pi f(t-\tau)] + a_{2k}\sin[2\pi f(t-2\tau)] \\ &\quad + \ldots + a_{Mk}\sin[2\pi f(t-M\tau)]\}dt \\ &= a_{0k}r_{00} + a_{1k}r_{01} + \ldots + a_{Mk}r_{0M}, \end{aligned} \quad (3)$$

where

$$\begin{aligned} r_{0m} &= \int_0^T \sin(2\pi ft) \times \sin[2\pi f(t-m\tau)]dt. \\ &\quad (m = 0, \ldots, M) \end{aligned} \quad (4)$$

(3) is a linear equation about all information bits. Then, sub-carriers with delay $m\tau$ $(m = 1, \ldots, M)$ are utilized in turn to implement the coherent operation with the received signal,

$$\begin{aligned} G_{mk} &= \int_0^T \sin[2\pi f(t-m\tau)] \times S_k(t)dt \\ &= \int_0^T \sin[2\pi f(t-m\tau)] \\ &\quad \times \{a_{0k}\sin(2\pi ft) + a_{1k}\sin[2\pi f(t-\tau)] \\ &\quad + a_{2k}\sin[2\pi f(t-2\tau)] + \ldots \\ &\quad + a_{Mk}\sin[2\pi f(t-M\tau)]\}dt \\ &= a_{0k}r_{m0} + a_{1k}r_{m1} + \ldots + a_{Mk}r_{mM}, \end{aligned} \quad (5)$$

where

$$\begin{aligned} r_{mn} &= \int_0^T \sin[2\pi f(t-m\tau)] \times \sin[2\pi f(t-n\tau)]dt. \\ &\quad (m = 1, \ldots, M, n = 0, \ldots, M) \end{aligned} \quad (6)$$

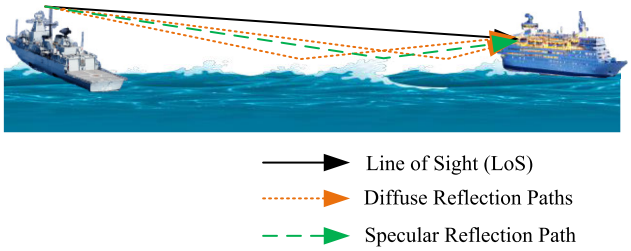

FIGURE 4. Maritime wireless channel model.

After $N = M+1$ coherent operations, an equation set about all information bits are constructed as

$$\boldsymbol{R}\boldsymbol{A}_k = \boldsymbol{G}_k, \tag{7}$$

where

$$\boldsymbol{R} = \begin{bmatrix} r_{00} & r_{01} & \dots & r_{0M} \\ r_{10} & r_{11} & \dots & r_{1M} \\ \vdots & \vdots & \ddots & \vdots \\ r_{M0} & r_{M1} & \dots & r_{MM} \end{bmatrix}, \tag{8}$$

$$\boldsymbol{A}_k = \begin{bmatrix} a_{0k} & a_{1k} & \dots & a_{Mk} \end{bmatrix}^T, \tag{9}$$

$$\boldsymbol{G}_k = \begin{bmatrix} G_{0k} & G_{1k} & \dots & G_{Mk} \end{bmatrix}^T. \tag{10}$$

Then, all the information bits are obtained through soling (7),

$$\boldsymbol{A}_k = \boldsymbol{R}^{-1}\boldsymbol{G}_k. \tag{11}$$

After β clock cycles, the matrix of chaotic reference signal and information bearing signals can be obtained and expressed as:

$$X = \begin{bmatrix} x_1 & x_2 & \dots & x_\beta \end{bmatrix}, \tag{12}$$

$$Y = \begin{bmatrix} s_1x_1 & s_1x_2 & \dots & s_1x_\beta \\ s_2x_1 & s_2x_2 & \dots & s_2x_\beta \\ \vdots & \vdots & \ddots & \vdots \\ s_Mx_1 & s_Mx_2 & \dots & s_Mx_\beta \end{bmatrix}, \tag{13}$$

Finally, the data are obtained through matrix multiplying:

$$\hat{\boldsymbol{s}} = \begin{bmatrix} \hat{s}_1 & \hat{s}_2 & \dots & \hat{s}_M \end{bmatrix} = \text{sign}\left(X \cdot Y'\right). \tag{14}$$

where the symbol "^" represents the recovered bits at the receiver.

B. MARITIME WIRELESS CHANNEL MODEL

As there are little obstacles in the maritime environment, the main propagation path of the signal is line of sight (LoS). However, due to the wind and waves in the sea, there always exists surface fluctuations, thus reflections by the sea surface must be considered when the sea state is rough. According to Fig. 4, the model of the maritime communication channel is always based on the two-ray model, which contains the LoS path and various reflection path including one specular reflection path and multiple diffuse paths. All reflection paths are distributed in the "effective reflection region".

According to [22], the strength of the signal passing the specular reflection path relative to that of the signal passing the LoS path is

$$\frac{V_{\text{Specular}}}{V_{\text{LoS}}} = \rho_s\sqrt{G_{\text{ant}}}\,|\Gamma_v|\,\rho_{\text{veg}}, \tag{15}$$

where V_{Specular} and V_{LoS} represents the voltage of the signal passing the specular reflection path and the LoS path, respectively. In this paper, the relative antenna gain G_{ant} and the vegetation factor ρ_{veg} are both set to be 1 [22]. ρ_s is the specular reflection coefficient, Γ_v is the Fresnel reflection coefficient, and they can be expressed as:

$$\rho_s = \exp\left[-2\left(\frac{2\pi\sigma_h \sin(\varphi)}{\lambda}\right)^2\right], \tag{16}$$

$$\Gamma_v = \frac{\varepsilon_c \sin\varphi - \sqrt{\varepsilon_c - \cos^2\varphi}}{\varepsilon_c \sin\varphi + \sqrt{\varepsilon_c - \cos^2\varphi}}. \tag{17}$$

where σ_h is the rms surface hight variation, φ is the grazing angle, λ is the wavelength, and ε_c is the surface dielectric constant. σ_h depends on the roughness of the sea state. For instance, σ_h equals to 0.3 m in the gentle sea state [22].

What's more, the strength of the signal passing the diffuse reflection path relative to that of the signal passing the LoS path is [22]

$$\frac{V_{\text{Diffuse}}}{V_{\text{LoS}}} = \sqrt{\frac{1}{4\pi}\left(\frac{R}{R_1R_2}\right)^2\frac{1}{\beta_0^2}\exp\left(-\frac{\beta^2}{\beta_0^2}\right)dA} \cdot |\Gamma_v| \cdot \rho_{\text{veg}} \cdot \sqrt{G_{\text{ant}}} \cdot \rho_{\text{roughness}} \cdot \sqrt{S_f}. \tag{18}$$

where R represents the distance of the LoS path, and R_1 and R_2 represents the distance from the transmitter to the reflection point and from the reflection point to the receiver, respectively. In this paper, R is set to be 5 km, and R_1 and R_2 are set to be 100 m and 10 m, respectively. β_0 represents the angle between the bisector of the R_1 and R_2 rays and the local vertical, and β is the mean square value of the surface slope over the region of interest. $\rho_{\text{roughness}}$ is the roughness factor, $\sqrt{S_f}$ is the shadowing factor, and dA is an arbitrary small patch of area lying on the effective reflection region.

In addition, according to the standard [23], most reflections occur in the first 10.4 μs of the signal. Thus, in this paper, all the multi-path time delays are set to be less than 10.4 μs.

III. PERFORMANCE ANALYSIS

A. SPECTRAL EFFICIENCY

The most remarkable characteristic of SCDS-DCSK is its high spectral efficiency. As all sub-carriers have the same frequency, the SCDS-DCSK symbol only occupies the bandwidth of a single frequency sub-channel, as shown in Fig. 5. According to the standard [23], the symbol rate of a VHF system is 2400 symbols/s, which means that the bandwidth of one frequency sub-channel is 4.8 kHz. In VDES, the frequency interval between neighbor sub-channels is 2.7 kHz, indicating that the frequency sub-channels are not orthogonal. Thus, the bandwidth of a VDES symbol is wide. For

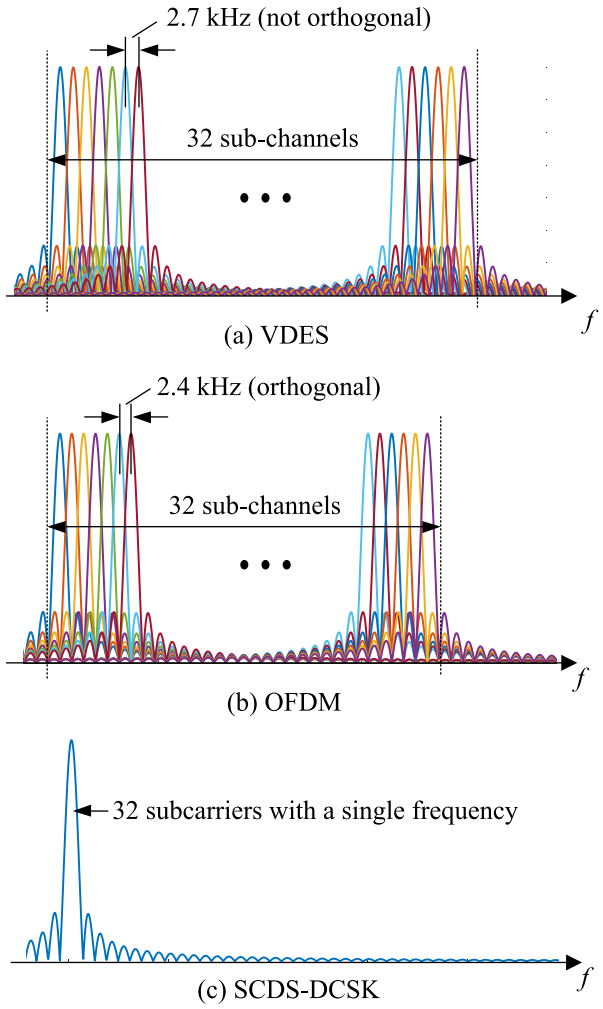

FIGURE 5. Spectrum of VDES, OFDM and SCDS-DCSK.

OFDM, sub-channels are orthogonal with each other, and the frequency interval of neighbor sub-channels is 2.4 kHz. Thus, the bandwidth of an OFDM symbol is narrower than that of VDES. However, despite the spectrums of sub-carriers are overlapped, OFDM still occupies a certain bandwidth, as shown in Fig. 5(b). In SCDS-DCSK, all sub-carriers are gathered into a single frequency sub-channel. As a result, the spectrum of SCDS-DCSK is much narrower than the above two multi-carrier modulation technologies, and the spectral efficiency can be significantly increased. Therefore, a large amount of spectrum resources is saved, and more communication nodes can be allowed to access the maritime IoV communication network.

Let the total number and duration of the sub-carrier be N and T, respectively, and the bandwidth of one sub-carrier is $2/T$. Symbol durations of VDES and OFDM are both T, and the frequency interval are $2.7/2.4^*(1/T)$ and $(1/T)$, respectively. Assuming that each sub-channel carries N_b bits, the data rate of VDES and OFDM is

$$R_{\text{VDES}} = R_{\text{OFDM}} = \frac{(N-1)\cdot N_b}{\beta T} \tag{19}$$

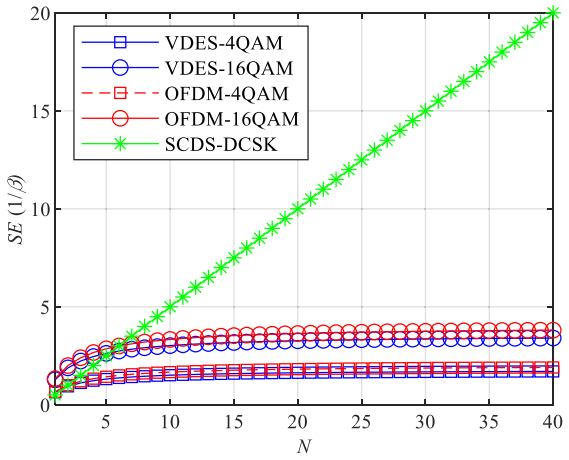

FIGURE 6. Spectral efficiency of VDES, OFDM and SCDS-DCSK. For 4-QAM modulation, $N_b = 2$. For 16-QAM modulation, $N_b = 4$. For SCDS-DCSK, $N_b = 2$.

Then, the bandwidth and spectral efficiency of VDES and OFDM can be respectively expressed as:

$$B_{\text{VDES}} = (N-1)\cdot\frac{2.7}{2.4}\cdot\frac{1}{T} + 2\cdot\frac{1}{T}, \tag{20}$$

$$\begin{aligned} SE_{\text{VDES}} &= R_{\text{VDES}}/B_{\text{VDES}} \\ &= \frac{(N-1)\cdot N_b/\beta T}{(N-1)\cdot\frac{2.7}{2.4}\cdot\frac{1}{T} + 2\cdot\frac{1}{T}} \\ &= \frac{(N-1)\cdot N_b}{\beta\left[(N-1)\cdot\frac{2.7}{2.4} + 2\right]}. \end{aligned} \tag{21}$$

$$B_{\text{OFDM}} = (N+1)\cdot\frac{1}{T}, \tag{22}$$

$$SE_{\text{OFDM}} = R_{\text{OFDM}}/B_{\text{OFDM}} = \frac{(N-1)\cdot N_b}{(N+1)\cdot\beta}. \tag{23}$$

For SCDS-DCSK, the duration of one symbol is $2T$, and the bandwidth is same with that of a single sub-carrier, i.e., $2/T$.

Therefore, the spectral efficiency can be expressed as:

$$\begin{aligned} SE_{\text{SCDS-DCSK}} &= \frac{R_{\text{SCDS-DCSK}}}{B_{\text{SCDS-DCSK}}} = \frac{\frac{(N-1)\cdot N_b}{2\beta T}}{2\cdot\frac{1}{T}} \\ &= \frac{(N-1)\cdot N_b}{4\beta}. \end{aligned} \tag{24}$$

Fig. 6 shows the spectral efficiency of VDES, OFDM and SCDS-DCSK. For the first two technologies, the spectral efficiency tends to reach a specific upper limit. However, the spectral efficiency of SCDS-DCSK is a linear function about the total number of subcarriers. When N is bigger than 8, the spectral efficiency of SCDS-DCSK begins to be larger than the rest two competitors. This gap becomes larger when N increases. Thus, the proposed SCDS-DCSK can significantly increase the spectral efficiency of the communication system.

B. PAPR

In traditional multi-carrier modulations, the phases of all sub- carriers are the same. As a result, a high PAPR may be triggered during the construction of a symbol, and

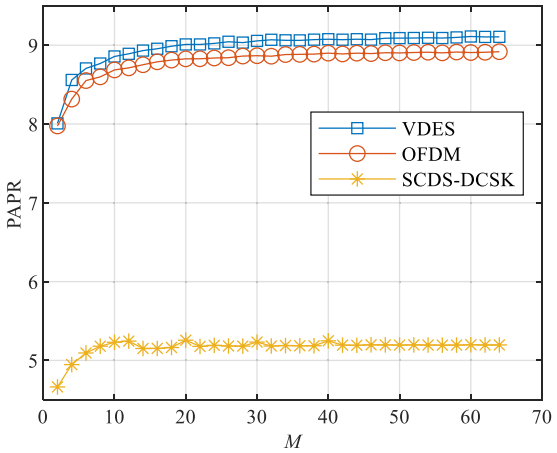

FIGURE 7. PAPR of VDES, OFDM and SCDS-DCSK. The calculation of PAPR is similar to [24].

a high PAPR will induce a higher receiver complexity. In SCDS-DCSK, the sub-carriers are delayed in turn in time domain, then amplitude offsets will occur during symbol construction, indicating a lower PAPR. From Fig. 7, the PAPR of SCDS-DCSK is nearly half of that of VDES and OFDM. Thus, SCDS-DCSK has a lower PAPR than existing multi-carrier modulation technologies.

C. COMPLEXITY

In this paper, the total number of multiplications and additions is used to define the complexity. As the transmitter of SCDS-DCSK is similar with a MC-DCSK system, the complexity of the transmitter is the same as that of the traditional MC-DCSK, and they both need N multiplications and $(N-1)$ additions to form a symbol at the transmitter. However, the complexity of the receiver of SCDS-DCSK is higher than that of the traditional MC-DCSK. For the traditional MC-DCSK, N multiplications are needed to demodulate the information bits. For SCDS-DCSK, N multiplications are needed firstly to implement N coherent operations, and the complexity of solving a linear equation set is $O(N^3)$. Thus, SCDS-DCSK pays a price of increasing the complexity to increase the spectral efficiency. However, as the maritime spectrum resource is very limited, it is worth to pay the price of complexity to save the resources.

D. BER ANALYSIS

Firstly, the origin of BER is analyzed under additional Gaussian white noise (AWGN) channel. The signal passing the AWGN channel can be expressed as

$$\boldsymbol{r}_k = \boldsymbol{s}_k + \boldsymbol{n}_k, \tag{25}$$

where $\boldsymbol{r}_k$, $\boldsymbol{s}_k$ and $\boldsymbol{n}_k$ represent the received signal, transmitted signal and noise in the channel, respectively. Then, the coherent operation changes into

$$\boldsymbol{C}^T\boldsymbol{r}_k = \boldsymbol{C}^T\left(\boldsymbol{s}_k + \boldsymbol{n}_k\right) = \boldsymbol{C}^T\boldsymbol{s}_k + \boldsymbol{C}^T\boldsymbol{n}_k = \boldsymbol{G}_k + \Delta\boldsymbol{G}_k. \tag{26}$$

where $\boldsymbol{C} = [g_0(t), g_1(t), \ldots, g_M(t)]$ represents the matrix of all sub-carriers. $\Delta\boldsymbol{G}$ represents the deviation of the coherent operation induced by the noise n_k. As a result, (7) becomes

$$\boldsymbol{R}\left(\boldsymbol{A} + \Delta\boldsymbol{A}\right) = \boldsymbol{G} + \Delta\boldsymbol{G}, \tag{27}$$

where $\Delta\boldsymbol{A}$ represents the error vector of the solution. A large $\Delta\boldsymbol{A}$ will cause a bigger error of the matrix multiplex (10), and then cause a high BER. As $RA \equiv G$, we have

$$\boldsymbol{R}\Delta\boldsymbol{A} = \Delta\boldsymbol{G}, \tag{28}$$

Therefore, we have

$$\Delta\boldsymbol{A} = \boldsymbol{R}^{-1}\Delta\boldsymbol{G}. \tag{29}$$

According to the properties of the norm, we have

$$\|\Delta\boldsymbol{A}\| \le \left\|\boldsymbol{R}^{-1}\right\| \cdot \|\Delta\boldsymbol{G}\|. \tag{30}$$

From (30), the norm of $\Delta\boldsymbol{A}$ depends not only on the noise, but also on the norm of $\boldsymbol{R}^{-1}$. If the norm of $\boldsymbol{R}^{-1}$ is large, the error of the solution will further increase, and the BER will consequently increase. According to (4) and (6), elements of $\boldsymbol{R}$ is obtained through coherent operations between subcarriers. Therefore, the parameter of subcarriers, such as the frequency f, the total number N, or even the form of the subcarriers (sinusoidal or cosine) will affect the BER of SCDS-DCSK. To guarantee the performance, parameters of subcarriers must be chosen appropriately to ensure a smaller $\left\|R^{-1}\right\|$.

Then, the BER expression of the SCDS-DCSK under an additive white Gaussian noise (AWGN) channel model is derived to analyze the system performance in the LoS path. At the receiver, the demodulated information matrix is

$$D = \begin{bmatrix} x_1 + \Delta x_1 & \cdots & x_\beta + \Delta x_\beta \\ s_1x_1 + \Delta s_1x_1 & \cdots & s_1x_\beta + \Delta s_1x_\beta \\ \vdots & \ddots & \vdots \\ s_Mx_1 + \Delta s_Mx_1 & \cdots & s_Mx_\beta + \Delta s_Mx_\beta \end{bmatrix} \tag{31}$$

Therefore, the decision variable for the mth bit is

$$\begin{aligned} B_m &= \sum_{k=1}^{\beta}\left(s_mx_k + \Delta\left(s_mx_{ku}\right)\right) \times \left(x_k + \Delta x_k\right) \\ &= \sum_{k=1}^{\beta} s_mx_kx_k + \sum_{k=1}^{\beta}\left(s_mx_k \cdot \Delta x_k + x_k \cdot \Delta\left(s_mx_k\right)\right) \\ &\quad + \sum_{k=1}^{\beta}\left(\Delta\left(s_mx_k\right) \cdot \Delta x_k\right). \end{aligned} \tag{32}$$

Here we consider $\sum_{k=1}^{\beta} x_kx_i \approx 0$. Meanwhile, Eq. (29) is

$$\Delta\boldsymbol{A} = \boldsymbol{R}^{-1}\Delta\boldsymbol{G} = \boldsymbol{R}^{-1}\boldsymbol{C}\boldsymbol{n} = \boldsymbol{V}\boldsymbol{n}. \tag{33}$$

where $\boldsymbol{C} = \begin{bmatrix} g_0(t) & g_1(t) & \cdots & g_{M-1}(t) & g_M(t) \end{bmatrix}^T$. Thus, we have

$$\Delta x_k = \sum_{t=1}^{T} V(t)\, n_t, \tag{34}$$

$$\Delta\left(s_m x_k\right) = \sum_{t=1}^{T} V\left(t\right) n_t. \tag{35}$$

The above two variables should have a similar statistical distribution with the additive Gaussian noise. As one chaotic reference signal is shared by multiple information bits, the expectation and variance of the decision variable of the mth sub-carrier is

$$E\left(B_m \left| a_m = +1\right.\right) = \frac{M+1}{M} E_b, \tag{36}$$

$$\text{var}\left(B_m\right) = \frac{M+1}{M} E_b \frac{N_0}{2} \times \left[\left(\sum_{t=1}^{T} V\left(1,t\right)\right)^2 + \left(\sum_{t=1}^{T} V_b\left(m,t\right)\right)^2\right]. \tag{37}$$

where $E_b = \sum_{k=1}^{\beta} x_k^2$ Finally, the BER expression is (38), as shown at the bottom of the next page.

E. CHANNEL ESTIMATION AND EQUALIZATION IN MARITIME MULTI-PATH CHANNEL

As there are already time delays in the symbol of SCDS-DCSK, the additional time delay induced by the maritime multi-path channel will bring a huge interference to the equation set. Therefore, the performance of SCDS-DCSK will suffer a severe deterioration under the multi-path channel. To ensure the performance of SCDS-DCSK, a channel estimation and equalization method is designed. However, in the proposed SCDS-DCSK, a simpler channel estimation and equation method can be implemented, which does not need any channel coefficient.

Firstly, a pilot that is composed by unmodulated subcarriers is inserted in front of the symbol,

$$s_{Pilot}\left(t\right) = \sum_{s=0}^{M} \sin\left[2\pi f_u\left(t - s\cdot\tau\right)\right], \quad t \in [0, T] \tag{39}$$

Then, the channel model is obtained by the pilot,

$$H = \frac{FFT\left(\hat{s}_{Pilot}\left(t\right)\right)}{FFT\left(s_{Pilot}\left(t\right)\right)} \tag{40}$$

where $\hat{s}_{Pilot}\left(t\right)$ represents the received pilot signal, and $FFT()$ is the fast Fourier transform process. Finally, the channel equalization is implemented using the channel model,

$$r\left(t\right) = IFFT\left(\frac{FFT\left(\hat{s}\left(t\right)\right)}{H}\right) \tag{41}$$

where $\hat{s}\left(t\right)$ is the received communication symbol, and IFFT() is the inverse fast Fourier transform process.

TABLE 1. Meanings of system parameters in simulation.

Symbol	Meaning	Value
β	Spreading factor	10, 20, 40
f	Frequency of the sub-carrier (Number of periods)	1, 2, 3, 4, 5
N	Total number of sub-carriers	16, 32, 48, 64
st	Level of the sea state	2, 4, 5, 6, 7, 8

TABLE 2. The norm of R^{-1} for various frequencies of subcarriers.

f	$\left\|\boldsymbol{R}^{-1}\right\|$
1	20.0049
2	4.8864
3	2.0879
4	1.1100
5	0.6589

IV. SIMULATION RESULTS AND DISCUSSIONS

A. EFFECTS OF SYSTEM PARAMETERS ON THE SYSTEM PERFORMANCE

In this subsection, effects of various parameters on the system performance are discovered. The meanings of main symbols during simulation are summarized in Table 1.

As a basic parameter of the spectrum-spreading system, the spreading factor β represents the length of the chaotic sequence, and its effect on the system performance is explored at first. From Fig. 8 (a) and (b), the BER performance is inversely proportional to β, i.e., the larger β is, the higher BER is. According to [12], a longer chaotic sequence will bring more noise samples into the receiver, causing more interferences to the decision module in the receiver. However, a longer chaotic sequence can enhance the level of the security. Thus, there is a tradeoff between the system performance and the spreading factor β. In the rest of this paper, β is set to be 10 to ensure the system performance.

According to the analyses in the last section, the parameter of the sub-carrier will affect the norm of $\boldsymbol{R}^{-1}$, and then affect the performance of SCDS-DCSK. Obviously, changing the frequency of the sub-carrier will influence the form of sub-carriers and then affect the system performance. In this manuscript, the parameter f denotes the number of periods in a fixed time duration T. For instance, in Fig. 8, the frequencies of subcarriers are set to be 1, i.e., there is only one period in the duration T. When f is larger than 1, there is more than one periods in the duration T. Fig. 9 shows the effect of the frequency f on the system performance. The system performa-nce is improved when f increases. Table 2 gives norms of $\boldsymbol{R}^{-1}$ for various f, and a larger f will bring a smaller $\left\|R^{-1}\right\|$ and a better system performance. This verifies the theoretical analysis in the last section. Thus, increasing the frequency of the subcarrier is an effective way to improve the performance of SCDS-DCSK.

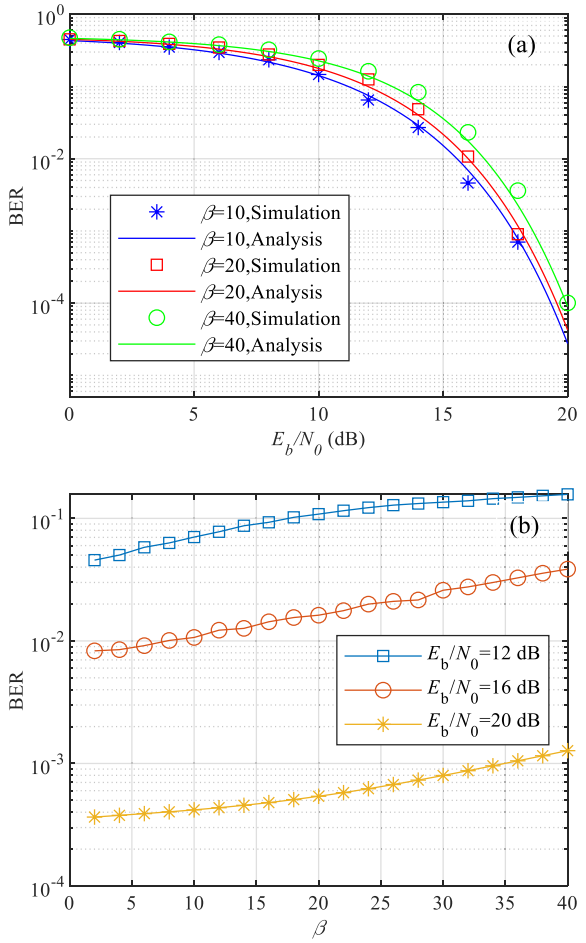

FIGURE 8. Effect of the spreading factor β on the system performance. (a) BER performance of SCDS-DCSK for various β. (b) BER performance versus β for various SNR values.

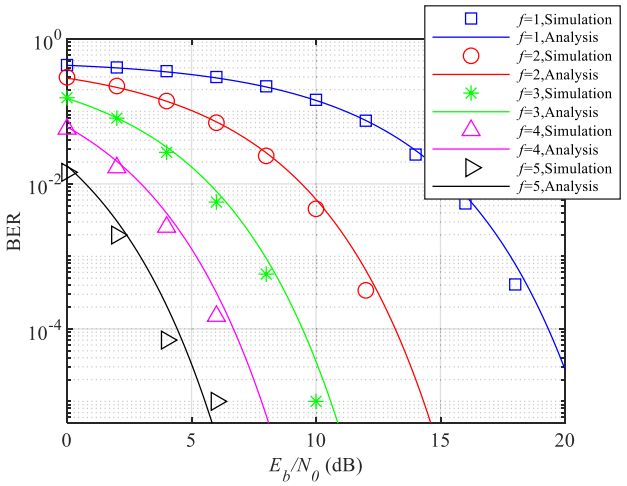

FIGURE 9. Effect of the subcarrier frequency on the system performance.

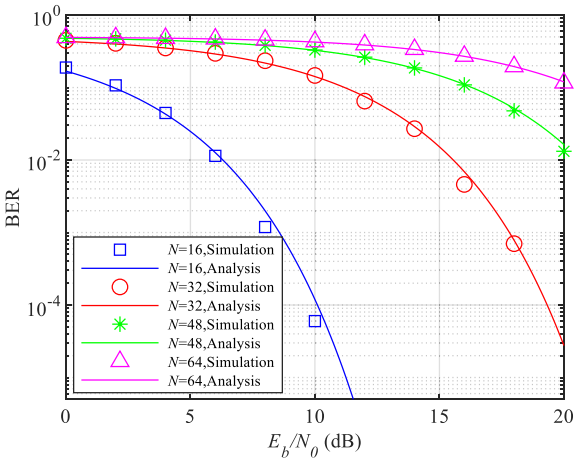

FIGURE 10. Performance of SCDS-DCSK under various N.

What's more, the total number of subcarriers N decides the dimension of $\boldsymbol{R}$ and $\boldsymbol{R}^{-1}$, and can also affect the system performance. From Fig. 10, the BER performance is the best when N equals to 16, and the performance deteriorates when N increases. The norm of $\boldsymbol{R}^{-1}$ in Table 3 reveals this law, i.e., a larger N makes a bigger norm of $\boldsymbol{R}^{-1}$, and the BER is higher. However, according to (24), reducing N will decrease the spectral efficiency. Thus, there is also a tradeoff between the system performance and the spectral efficiency. In the standard [23], 32 sub-channels are required to achieve the peak data transmission rate 307.2 kbps. Thus, to be fair, unless specifically mentioned, the total number of subcarriers N of SCDS-DCSK is also set to be 32.

In addition, SCDS-DCSK with $N = 48$ and 64 means a much higher spectral efficiency than existing technologies. However, the system performance also significantly

$$
\begin{aligned}
BER &= \sum_{m=1}^{M} BER_m \\
&= \sum_{m=1}^{M} \frac{1}{2} erfc \left\{ \left[\frac{M+1}{M} \left[\left(\sum_{t=1}^{T} V(1,t) \right)^2 + \left(\sum_{t=1}^{T} V(m,t) \right)^2 \right] \frac{N_0}{E_b} \right. \right. \\
&\quad \left. \left. + \left(\frac{M+1}{M} \left[\left(\sum_{t=1}^{T} V(1,t) \right)^2 + \left(\sum_{t=1}^{T} V(m,t) \right)^2 \right] \right)^2 \frac{\beta}{2} \left(\frac{N_0}{E_b} \right)^2 \right]^{-\frac{1}{2}} \right\}
\end{aligned} \tag{38}
$$

TABLE 3. The norm of R^{-1} for various N.

N	$\left\|\boldsymbol{R}^{-1}\right\|$
16	2.3671
32	20.0049
48	75.0416
64	177.7859

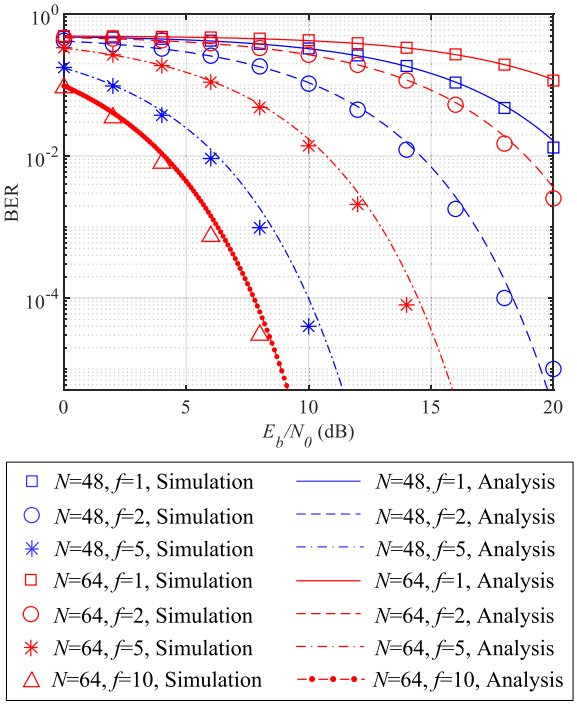

FIGURE 11. System performance of SCDS-DCSK with $N = 48$ and 64. For $N = 48$, f =1, 2, 5; for $N = 64$, f = 1, 2, 5 and 10.

TABLE 4. Norms of R^{-1} for N = 48 and 64.

f	$\left\|\boldsymbol{R}^{-1}\right\|$	
	N=48	N=64
1	75.0416	177.7859
2	13.7099	36.9407
5	2.0369	5.6913
10	0.3807	1.2352

deteriorates. To improve these performances, the BER of $N = 48$ and 64 with f larger than 1 is evaluated. Form Fig. 11, we can see that the system performance is improved when f increases, and the norm of $\boldsymbol{R}^{-1}$ in Table 4 also match with this result. Therefore, to simultaneously get a higher spectral efficiency and a good system performance, the frequency of sub-carriers should be larger than 1. What's more, from Fig. 7 to Fig. 10, simulation results match well with theoretical curves, indicating that the theoretical analysis is correct.

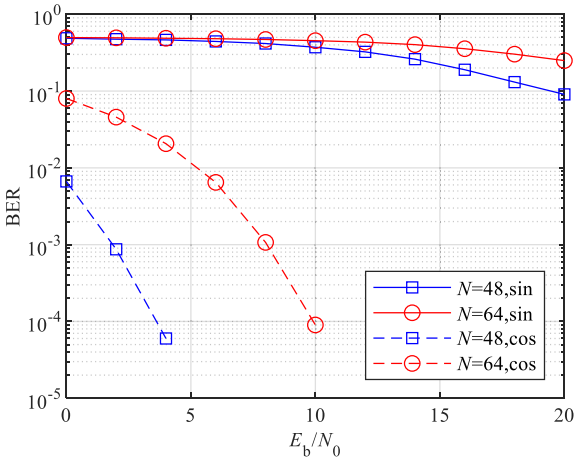

FIGURE 12. Performances of SCDS-DCSK under various sea states. $N = 32$, and $f = 1$.

TABLE 5. Norms of R^{-1} for sinusoidal and cosine-carriers.

N	$\left\|\boldsymbol{R}^{-1}\right\|$	
	sin	cos
48	75.0416	0.0996
64	177.7859	0.1331

TABLE 6. Main parameters during simulations.

Level of sea state (st)	σ_h (m)	Total number of diffuse reflection paths	Strength of diffuse reflection paths relative to LoS (dB)
2	0.3	2	-20
4	1.8	3	-15
5	2.4	4	-11.5
6	4.3	6	-10
7	7.62	8	-7
8	13.72	10	-5

Finally, Fig. 12 shows the system performance of SCDS-DCSK with cosine sub-carriers. We can see that the SCDS-DCSK with the cosine sub-carrier has a better BER performance than SCDS-DCSK with the sinusoidal sub-carrier. This phenomenon can be verified by the norm of $\boldsymbol{R}^{-1}$, which is shown in Table 5. When the sub-carrier is cosine type, the norm of $\boldsymbol{R}^{-1}$ is much smaller than the SCDS-DCSK with the sin-type sub-carrier. As analyzed in section III, the system performance of SCDS-DCSK is proportional to the norm of $\boldsymbol{R}^{-1}$, the SCDS-DCSK with the cosine type sub-carrier therefore has a better performance. In this way, utilizing cosine sub-carriers is another way to improve the performance of SCDS-DCSK.

B. EFFECTS OF SEA STATES ON THE SYSTEM PERFORMANCE

Above results are under the assumption that the sea state is relatively gentle. In this subsection, the performance of

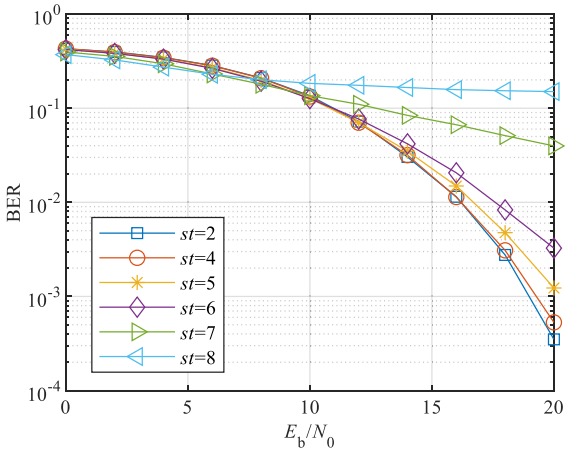

FIGURE 13. Performances of SCDS-DCSK with various f under diverse sea states. (a) Performance of SCDS-DCSK for various f under level 4, 5 and 6 sea states. (b) Performance of SCDS-DCSK for various f under level 7 and 8 sea states.

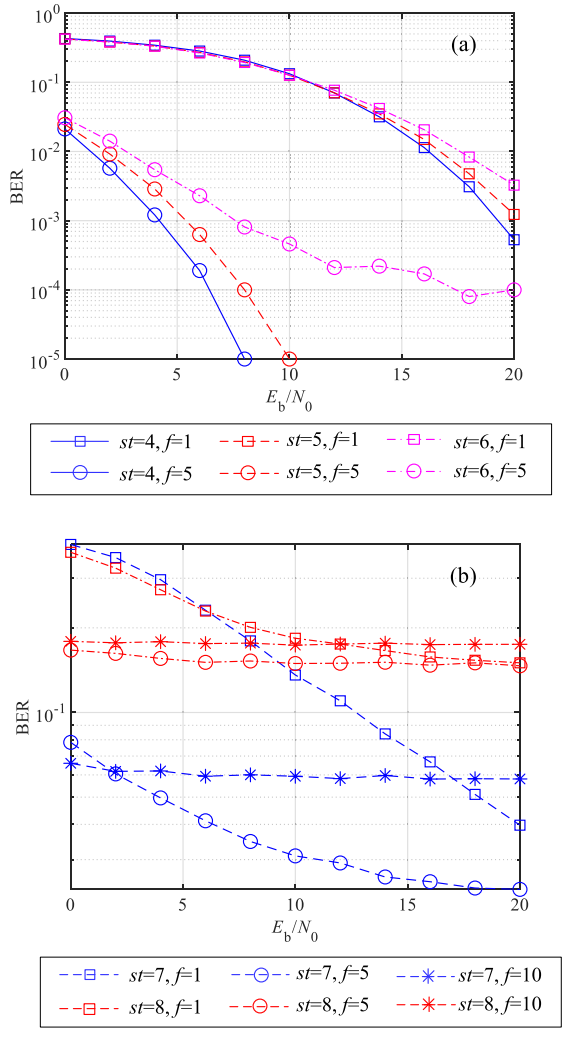

FIGURE 14. Performances of SCDS-DCSK with cosine sub-carriers under level 7 and 8 sea states.

SCDS-DCSK under various sea states is evaluated. According to [22] and [25], main parameters during simulations

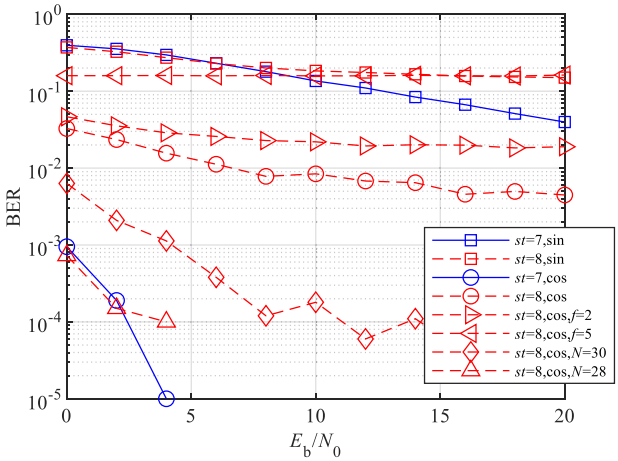

FIGURE 15. BER comparison between SCDS-DCSK and (a) MC-DCSK and (b-c) OFDM-DCSK. (a) BER comparison between SCDS-DCSK and MC-DCSK. (b) BER comparison between SCDS-DCSK and OFDM-DCSK. The frequency of subcarriers of SCDS-DCSK is 1. (c) BER comparison between SCDS-DCSK and OFDM-DCSK. The frequency of subcarriers of SCDS-DCSK is 5.

are shown in Table 6. When the sea state becomes rough, there are more diffuse reflection paths and the delay of each reflection path becomes more random. Therefore, during simulation, when st is large, we add more diffuse reflection paths and the delay of each path is randomly set. What's more, the strength of diffuse reflection paths relative to LoS is calculated by (18).

In Fig. 13, the performances of BER under gentle sea states are similar, such as level 2 and level 4. When the level of the sea state enhances to level 5 and 6, the performance becomes worse. Especially, when the sea state becomes more and more rough, such as level 7 and 8, the BER maintains at 10^{-1}, which indicates that the communication fails. As increasing the frequency of the sub-carrier will improve the system performance, system performances under $f = 1, 5, 10$ are shown in Fig. 14. For sea states from level 2 to 6, the system performance is improved as f increases. However, for sea states at level 7 and 8, the BER still maintains at about 0.1 when f increases. This is due to the fact that the strength of all the diffuse reflections starts to be larger than that of the specular reflection. Thus, the multi-path interference becomes much more severe at high level of sea states.

To weaken the interference under high level of sea states, performances of SCDS-DCSK with cosine sub-carriers and various system parameters are explored. From Fig. 15, the system performance improves when subcarriers become cosine waveforms, especially at the sea state of level 7. This means that SCDS-DCSK with cosine subcarriers is more suitable for rough sea states. It is worth noting that, for level 8 sea state, increasing the frequency f deteriorates the performance. Thus, to ensure the system performance at level 8 sea state, N needs to be a little smaller, such as 30 or 28.

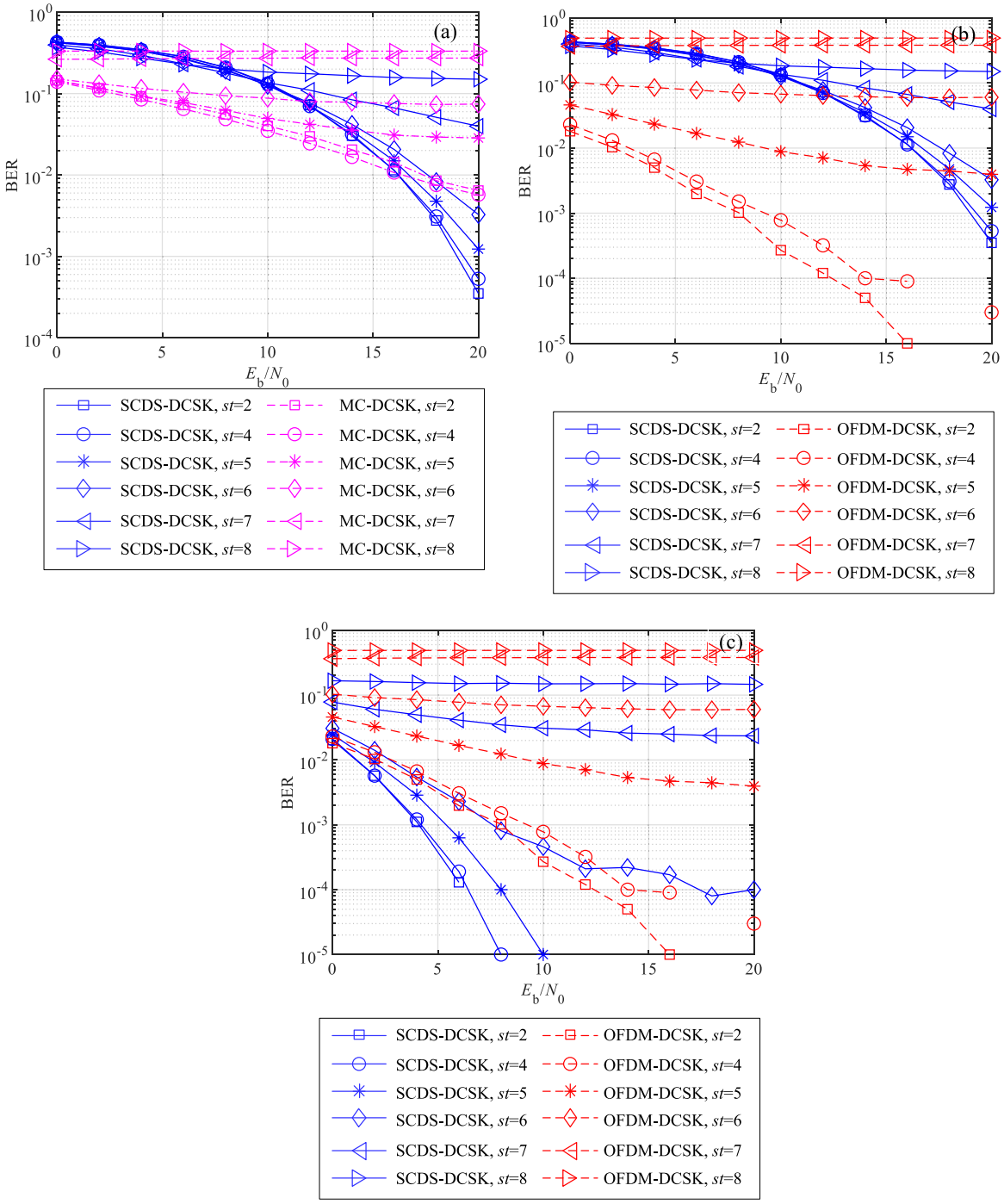

FIGURE 16. Performance of SCDS-DCSK with cosine sub-carriers.

C. COMPARISON WITH OTHER TYPICAL HIGH SPECTRAL EFFICIENCY DCSKS

In this sub-section, the performance of SCDS-DCSK is compared with other typical MC-DCSKs. As SCDS-DCSK increases the spectral efficiency from the aspect of basic modulations, comparisons are implemented between other DCSK systems with typical multi-carrier modulations, such as typical MC-DCSK and OFDM-DCSK. MC-DCSKs with index modulations are beyond the scope of comparison. In addition, simulations of all above technologies are based on the maritime communication channel in this paper.

From Fig. 16(a), for all sea states, performances of SCDS-DCSK are worse than that of the traditional MC-DCSK at low SNR region, and this relationship inverses at high SNR region. From Fig. 16(b), performances of OFDM-DCSK are better than that of SCDS-DCSK at

gentle sea states, such as level 2. For level 4 and 5, the performance of OFDM-DCSK begins to be worse than that of SCDS-DCSK at high SNR regions. For rougher sea states such as level 7 and 8, performance of SCDS-DCSK is also better than that of OFDM-DCSK at the high SNR region. When f increases to 5, the performance of SCDS-DCSK is better than that of OFDM-DCSK for all SNRs, as shown in Fig. 16(c).

V. DISCUSSION

From the simulation results, we can see that parameter of the proposed SCDS-DCSK system are highly flexible. For different performance requirements, SCDS-DCSK can provide various optimal parameter combinations. Firstly, the spreading factor can be set to 10 to ensure both the communication performance and the system reliability. Then, for gentle sea states, if the number of sub-channel is 32, which is the same as the VDES standard, the frequency of sub-carriers can be set to 1 to get a good communication performance. If a higher data transmission rate is required, such as N equals to 48 or 64, a higher sub-carrier frequency f such as 5 or 10 is needed to ensure the performance, or a cosine type sub-carrier is also an alternative. For rougher sea states such as level 5 or 6, a higher sub-carrier frequency f (5 for instance) is necessary. For the roughest sea state such as level 8, a cosine type sub-carrier with $N = 30$ or 28 and $f = 2$ is optimal for a better performance.

VI. CONCLUSION

In this paper, a single-carrier delay-and superposition based DCSK system is proposed and simulated under various system parameters and sea states. The results show that the proposed SCDS-DCSK can support the transmission of more than 32 paths of chaotic signals while only occupy the bandwidth of one single frequency sub-channel, indicating a significant improvement in terms of spectral efficiency. Meanwhile, under appropriate parameter settings, SCDS-DCSK can achieve high spectral efficiency data transmission at various sea states. Comparing with other typical MC-DCSK systems, the BER performance of the proposed SCDS-DCSK is better than that of the traditional MC-DCSK at high SNR region, and when the frequency of subcarriers is set to be 5, the BER performance of the proposed SCDS-DCSK is always better than OFDM-DCSK at various sea states. Therefore, SCDS-DCSK is a promising technology to improve the QoS of future maritime IoV. Future research can focus on fusing the index modulations with SCDS-DCSK to further improve the spectral efficiency, data rate and other performances.

REFERENCES

[1] Z. Wang and B. Lin, "Maritime internet of vessels," in *Encyclopedia of Wireless Networks*, X. Shen, X. Lin, and K. Zhang, Eds. Berlin, Germany: Springer, 2019, pp. 1–9. [Online]. Available: https://link.springer.com/referenceworkentry/10.1007/978-3-319-32903-1_344-1

[2] G. Cai, Y. Fang, P. Chen, G. Han, G. Cai, and Y. Song, "Design of an MISO-SWIPT-aided code-index modulated multi-carrier M-DCSK system for e-Health IoT," *IEEE J. Sel. Areas Commun.*, vol. 39, no. 2, pp. 311–324, Feb. 2021.

[3] G. Kaddoum, F. Richardson, and F. Gagnon, "Design and analysis of a multi-carrier differential chaos shift keying communication system," *IEEE Trans. Commun.*, vol. 61, no. 8, pp. 3281–3291, Aug. 2013.

[4] L. Wang, G. Cai, and G. R. Chen, "Design and performance analysis of a new multiresolution M-ary differential chaos shift keying communication system," *IEEE Trans. Wireless Commun.*, vol. 14, no. 9, pp. 5197–5208, Sep. 2015.

[5] H. Yang, W. K. S. Tang, G. Chen, and G.-P. Jiang, "System design and performance analysis of orthogonal multi-level differential chaos shift keying modulation scheme," *IEEE Trans. Circuits Syst. I, Reg. Papers*, vol. 63, no. 1, pp. 146–156, Jan. 2016.

[6] G. Cai, Y. Fang, G. Han, F. C. M. Lau, and L. Wang, "A square-constellation-based M-ary DCSK communication system," *IEEE Access*, vol. 4, pp. 6295–6303, 2016.

[7] T. Huang, L. Wang, W. Xu, and G. Chen, "A multi-carrier M-ary differential chaos shift keying system with low PAPR," *IEEE Access*, vol. 5, pp. 18793–18803, 2017.

[8] S. Li, Y. Zhao, and Z. Wu, "Design and analysis of an OFDM-based differential chaos shift keying communication system," *J. Commun.*, vol. 10, no. 3, pp. 199–205, Mar. 2015.

[9] G. Kaddoum, "Design and performance analysis of a multiuser OFDM based differential chaos shift keying communication system," *IEEE Trans. Commun.*, vol. 64, no. 1, pp. 249–260, Jan. 2016.

[10] G. Cheng, L. Wang, W. Xu, and G. Chen, "Carrier index differential chaos shift keying modulation," *IEEE Trans. Circuits Syst. II, Exp. Briefs*, vol. 64, no. 8, pp. 907–911, Aug. 2017.

[11] G. Cheng, L. Wang, Q. Chen, and G. Chen, "Design and performance analysis of generalised carrier index M-ary differential chaos shift keying modulation," *IET Commun.*, vol. 12, no. 11, pp. 1324–1331, Jun. 2018.

[12] G. Cai, Y. Fang, J. Wen, S. Mumtaz, Y. Song, and V. Frascolla, "Multi-carrier M-ary DCSK system with code index modulation: An efficient solution for chaotic communications," *IEEE J. Sel. Topics Signal Process.*, vol. 13, no. 6, pp. 1375–1386, Oct. 2019.

[13] X. Cai, W. Xu, L. Wang, and G. Kolumban, "Multicarrier M-ary orthogonal chaotic vector shift keying with index modulation for high data rate transmission," *IEEE Trans. Commun.*, vol. 68, no. 2, pp. 974–986, Feb. 2020.

[14] Y. Fang, G. Cai, G. Han, L. Wang, and P. Chen, "Performance analysis and comparison of three multiple-access DCSK cooperative communication systems over multipath fading channels," in *Proc. 17th Int. Symp. Commun. Inf. Technol. (ISCIT)*, Sep. 2017, pp. 1–5.

[15] G. Kaddoum, F.-D. Richardson, S. Adouni, F. Gagnon, and C. Thibeault, "Multi-user multi-carrier differential chaos shift keying communication system," in *Proc. 9th Int. Wireless Commun. Mobile Comput. Conf. (IWCMC)*, Jul. 2013, pp. 1798–1802.

[16] G. Kaddoum and F. Shokraneh, "Analog network coding for multi-user multi-carrier differential chaos shift keying communication system," *IEEE Trans. Wireless Commun.*, vol. 14, no. 3, pp. 1492–1505, Mar. 2015.

[17] H. Ma, G. Cai, Y. Fang, P. Chen, and G. Chen, "Design of a superposition coding PPM-DCSK system for downlink multi-user transmission," *IEEE Trans. Veh. Technol.*, vol. 69, no. 2, pp. 1666–1678, Feb. 2020.

[18] Z. Chen, L. Zhang, Z. Wu, L. Wang, and W. Xu, "Reliable and efficient sparse code spreading aided MC-DCSK transceiver design for multiuser transmissions," *IEEE Trans. Commun.*, vol. 69, no. 3, pp. 1480–1495, Mar. 2021.

[19] M. He, D. Liang, and Q. Cao, "A modulation with higher bandwidth efficiency than OFDM," in *Proc. ICSPS*, Dalian, China, Jul. 2010, pp. 393–397.

[20] Q. Cao and D. Liang, "Study on modulation techniques free of orthogonality restriction," *Sci. China F, Inf. Sci.*, vol. 50, no. 6, pp. 889–896, Dec. 2007.

[21] X. Cai, W. Xu, M. Miao, and L. Wang, "Design and performance analysis of a new M-ary differential chaos shift keying with index modulation," *IEEE Trans. Wireless Commun.*, vol. 19, no. 2, pp. 846–858, Feb. 2020.

[22] F. Huang, X. Liao, and Y. Bai, "Multipath channel model for radio propagation over sea surface," *Wireless Pers. Commun.*, vol. 90, no. 1, pp. 245–257, Sep. 2016.

[23] *Technical Characteristics for a VHF Data Exchange System in the VHF Maritime Mobile Band*, document ITU-R M. 2092-0, 2015.

[24] Z. Liu, L. Zhang, and Z. Chen, "Low PAPR OFDM-based DCSK design with carrier interferometry spreading codes," *IEEE Commun. Lett.*, vol. 22, no. 8, pp. 1588–1591, Aug. 2018.
[25] M. S. Choi, S. Park, Y. Lee, and S. R. Lee, "Ship to ship maritime communication for e-Navigation using WiMAX," *Int. J. Multimedia Ubiquitous Eng.*, vol. 9, no. 4, pp. 171–178, Apr. 2014.

XINYU DOU was born in Shenyang, Liaoning, China, in 1987. He received the B.S. degree in optical information science and technology and the Ph.D. degree in communication engineering from the Dalian University of Technology, Dalian, in 2010 and 2016, respectively.

From 2019 to 2021, he was a Postdoctoral Fellow of information and communication engineering at the Dalian Maritime University, China, where he is currently a Full Lecturer with the College of Information Science and Technology. His research interests include wireless communications, chaos-based wireless and optical communications, and neuromorphic photonics.

TENGXIAO LYU received the B.S. degree in communication engineering from Dalian Polytechnic University, Dalian, China, in 2019. He is currently pursuing the M.S. degree with the College of Information Science and Technology, Dalian Maritime University, Dalian. His research interests include maritime mobile communications and maritime edge calculations.

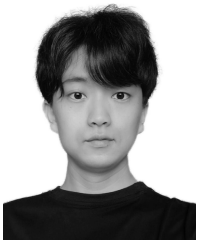

BAOJUN FAN received the B.S. degree in detection guidance and control technology from Shenyang Ligong University, Shenyang, China, in 2020. He is currently pursuing the M.S. degree with the College of Information Science and Technology, Dalian Maritime University, Dalian, China. His research interests include chaos-based digital communications and their applications to wireless communications.

DEQUN LIANG received the B.S. degree from Xi'an Jiaotong University, Xi'an, China, in 1966. From 1966 to 1998, he was a Full-Lecturer, a Full-Associate Professor, and a Full-Professor at Xi'an Jiaotong University. He was a Senior Visiting Scholar at the University of Manchester Institute of Science and Technology, from 1988 to 1989. From 1998 to 2011, he was a Full-Professor at the School of Information Science and Technology, Dalian Maritime University. He is the author of one book, more than 150 articles, and 14 patents. His research interests include wireless communications, pattern recognition, image processing, and artificial intelligence.